Main-Chain Fullerene Polymers for Photovoltaic Devices

Roger C. Hiorns,*,†,‡ Eric Cloutet,*,†,‡ Emmanuel Ibarboure,†,‡ Laurence Vignau,§ Noëlla Lemaitre,|| Stéphane Guillerez,|| Christelle Absalon,⊥ and Henri Cramail†,‡

CNRS, Laboratoire de Chimie des Polymères Organiques, 16 avenue Pey Berland, Pessac Cedex, F33607, France, Laboratoire de Chimie des Polymères Organiques, Université de Bordeaux, ENSCPB, Pessac Cedex, F33607, France, Laboratoire de l'Intégration du Matériau au Système, Université de Bordeaux, CNRS UMR 5218, ENSCPB, Pessac Cedex, F33607, France, INES CEA RDI - DTS/LCS, Le Bourget du Lac, F73370, France, and Centre d'Etude Structurale et d'Analyse des Molécules, Université de Bordeaux, Organiques, Talence Cedex, F33405, France

Received February 6, 2009; Revised Manuscript Received March 19, 2009

ABSTRACT: A prototype for a new class of macromolecules with a high fraction of fullerene is proposed. Their facile synthesis, modular structure, electronic activity, and novel solid-state behavior make them promising materials for photovoltaic applications. Controlled reversible-deactivation radical additions of the sterically bulky 1,4-bis(methylcyclohexyl ether)-2,5-dibromomethyl benzene to fullerene are indicated by GPC, NMR, and TGA studies to yield oligomers and polymers containing C_{60} in the main chain. UV and cyclic voltammetry indicate that the C_{60} undergoes mainly 1,4-additions and a minority (ca. 20%) of 1,2-additions to make a regio-irregular macromolecule. The same reaction performed in the presence of 1,4-bis(methylcyclohexyl ether)-2-bromomethyl benzene, resulting in macromolecules with bromomethyl-free chain ends, permitted confirmation of the aforementioned characteristics. The unusual reptation of the poly{(1,4-fullerene)-*alt*-[1,4-dimethylene-2,5-bis(cyclohexylmethyl ether)phenylene]}s (PFDP) in an Al/Ca/poly(3-hexylthiophene)-*blend*-PFDP/PEDOT-*blend*-PSS/ITO/glass structured device is demonstrated by AFM to yield nanoclusters at a scale (ca. 20 nm) favorable to exciton capture. Even without optimization of the chemical structure or the device, this prototype reached promising power conversion efficiencies of 1.6%.

Introduction

Polymer-based solar cells are expected to be market compliant due to their flexibility, lightweight nature, and low cost production.[1] Photovoltaic devices based on poly(3-hexylthiophene) (P3HT) and [6,6]-phenyl C_{61} butyric acid methyl ester (PCBM) have delivered efficiencies close to 5%.[2] Increased efficiencies are necessary to ensure their prevalent and pragmatic use. This will require the preparation of new classes of polymers that can be prepared with the minimum of synthetic steps.

In the dominant physical process the chromophore absorbs light to form an exciton that moves a mean distance[3] of around 10 nm. Charge formation results from the exciton at interfaces between the electron donor and acceptor. In the current best example, the polymeric nature of P3HT gives a mixture of amorphous zones, which enable close contact with PCBM, and crystalline zones, which permit long-range hole transport to the anode.[4,5] Intuitively, a polymeric acceptor should exhibit greater electron mobilities than small molecules over long distances due to covalent bonds and transport between acceptor groups that might extend throughout the photoactive layer. A polymeric acceptor may also form amorphous and crystalline domains to enhance exciton capture and electron transport, respectively. There is little work on polymeric acceptors when compared to the mass of literature on PCBM. The first example is that of a poly(phenylene vinylene) (PPV) cyano-derivative,[6,7] and more recently a sulfone-alkyl derivatized PPV.[8] For reasons not entirely understood though, polymers generally favor hole transport.[9] Commodity polymers that carry strong electron acceptors such as fullerene[10−12] or perylene[13] as pendent groups have been proposed to resolve this problem. However, the photovoltaic efficiencies are generally not as good as those for P3HT-*blend*-PCBM. There are various possible reasons for this, many based on device optimization, but questions concerning grafting densities and the incorporation of an electronically inert polymer backbone are relevant.

We therefore wished to simultaneously exploit the expected benefits of polymers and the electron acceptor properties of fullerene. This pointed us in the direction of main-chain fullerene polymers. There are examples in the literature, but they generally require multistep syntheses, can be "invasive" with respect to the electronic structure of the C_{60} due to the formation of multiple bonds, or result in insoluble products due to cross-linking.[14−17]

In polymer chemistry, chain ends are reacted with C_{60} using atom transfer radical addition (ATRA).[18,19] The chemistry is facile, and the paired addition ruptures only one double bond on the C_{60} sphere, thus retaining its aromatic structure. However, this methodology has not yet, to our knowledge, been adapted to the formation of high fullerene content polymers. We therefore wish to report an original adaptation of this reaction resulting in the preparation of poly{(1,4-fullerene)-*alt*-[1,4-dimethylene-2,5-bis(cyclohexylmethyl ether)phenylene]}s (PFDP), as shown in Scheme 1, along with the extremely novel behavior that these new materials exhibit in solid-state polymer-based photovoltaic devices.

Results and Discussion

The intermediate **4** was chosen to make C_{60}s proximate to enhance conductivity[9] and provide alkyl bromide groups for ATRA chemistry. It was prepared using well-established routes, and these are therefore detailed in the Supporting Information, along with NMRs confirming their structures (Figures S1−S3). It was expected that the bulky methylcyclohexyl ether groups

* To whom correspondence should be addressed. E-mail: roger.hiorns@neuf.fr (R.C.H.); cloutet@enscpb.fr (E.C.).
† CNRS.
‡ Laboratoire de Chimie des Polymères Organiques, Université de Bordeaux.
§ Laboratoire de l'Intégration du Matériau au Système, Université de Bordeaux.
|| INES CEA RDI - DTS/LCS.
⊥ Centre d'Etude Structurale et d'Analyse des Molécules, Université de Bordeaux.

10.1021/ma900279a CCC: $40.75
Published on Web 04/16/2009

Scheme 1. Synthetic Routes to PFDP 1 and PFDP 2[a]

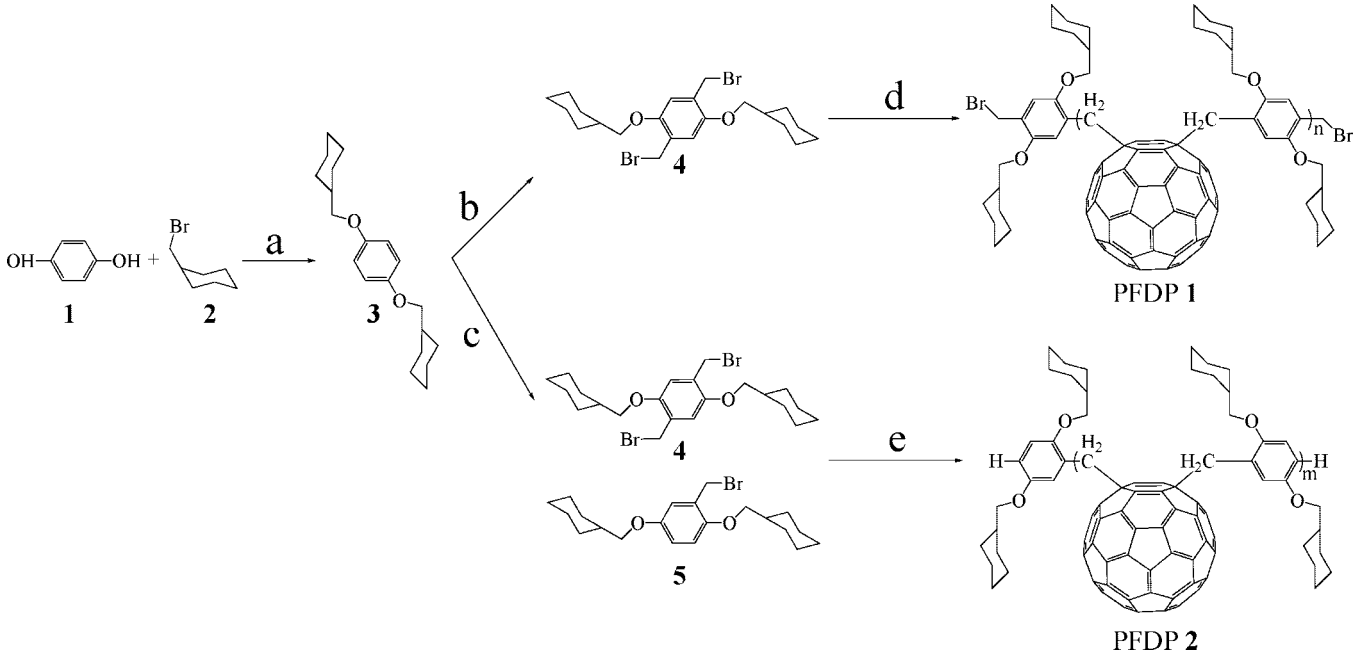

[a] (a) K_2CO_3, acetonitrile, 90 °C, 40 h; (b) paraformaldehyde, HBr, 65 °C, 80 min; (c) paraformaldehyde, HBr, 45 °C, 24 h; and (d and e) fullerene, CuBr, bipyridine, 22 h, 115 °C. For visual ease, only 1,4-bis addition products are shown.

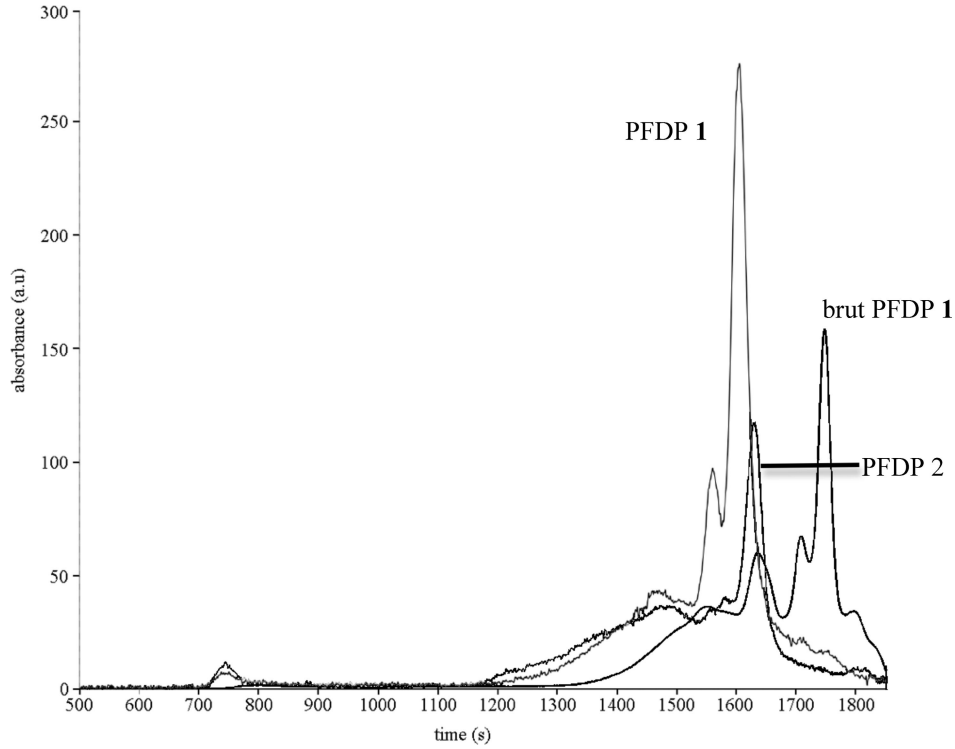

Figure 1. GPCs (THF, UV 254 nm) of PFDP **1**, PFDP **2**, and the brut product that led to PFDP **1**.

would ensure insertion of solvent between fullerenes and controlled additions to C_{60}. The latter reason is due to the stereoelectronic behavior of C_{60}; the steric nature of the incoming group strongly influences the point of addition around the sphere.[20] This was confirmed when an attempt to prepare a model compound using the small α-bromotoluene resulted in excessive and uncontrolled additions.

It could be imagined that to obtain PFDPs it would be best to start with equimolar amounts of C_{60} and dibrominated moieties (such as **4**). However, the number of radical additions to C_{60} is controlled by the ratio of $-CH_2Br$ groups and C_{60} in the reaction mixture.[18,19] If there are two or more $-CH_2Br$ groups to each C_{60}, then there is a risk of the C_{60} being tetra-substituted. Below this ratio, only two additions per C_{60} occur. To avoid the formation of an insoluble cross-linked product, the ratio of starting materials was 1.6 $-CH_2Br$ groups to 1 C_{60}. Reactions between CuBr reversibly deactivated $-CH_2Br$ groups are negligible due to the high electron acceptance of C_{60}. The purification of the resulting PFDPs was facilitated by their being soluble in THF, a nonsolvent of C_{60}.

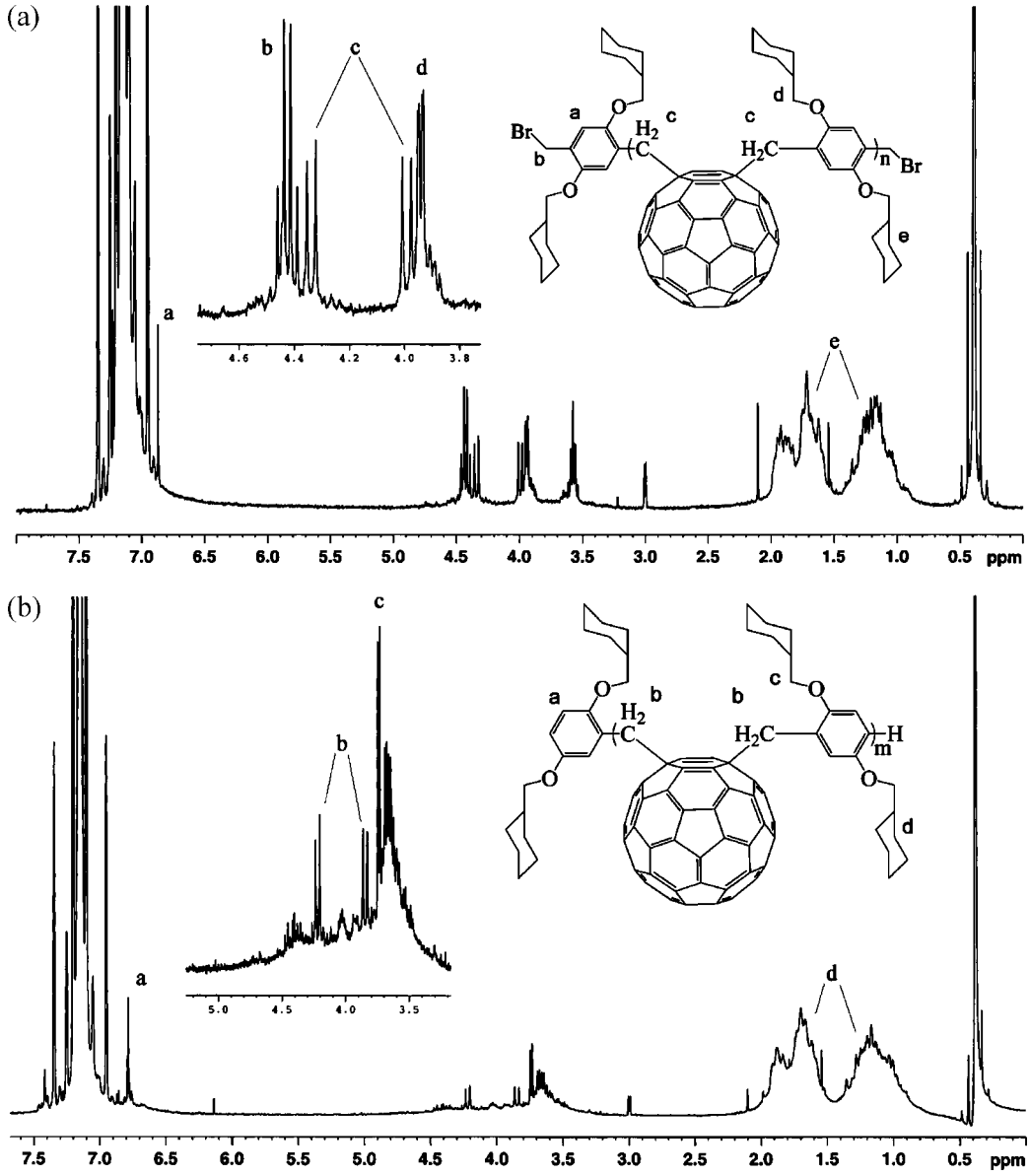

Figure 2. ^{1}H NMR spectra (C_6D_6, ambient) of (a) PFDP **1** and (b) PFDP **2**. Note that due to low concentration of PFDP and the propinquitous C_{60}s (that themselves have long relaxation times) and the long experiment times used (typically >48 h), minor peaks arise due to THF (m, 3.57; ca. 1.25 partially hidden by peaks due to cyclohexyl protons), methanol (3.00 ppm), toluene (2.10), acetone (1.54), and water (0.4 ppm), even though they are in extremely low concentrations.

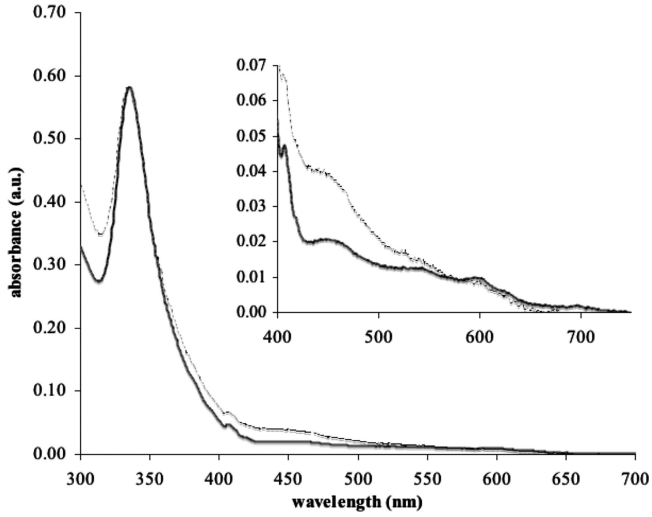

Figure 3. Normalized UV absorption characteristics of PFDP **1** (—) and PFDP **2** (- - -) in toluene with inset 10× zoom.

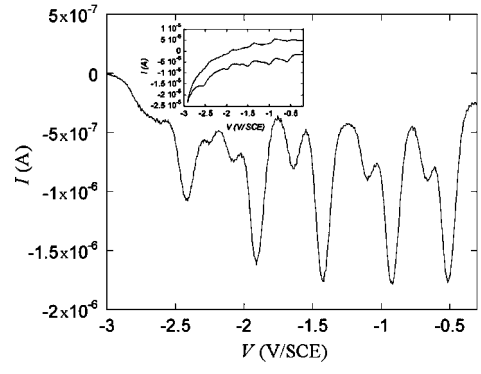

Figure 4. Representative pulse voltammogram of PFDP **2** in toluene/acetonitrile (4:1) at 25 °C in the presence of tetrabutylammonium hexafluorophosphate with inset cyclic voltammogram recorded under the same conditions.

A simple silica plug filtered out unreacted C_{60} and CuBr from a THF dispersion of the brut products.

To prepare a different but comparable polymer to verify the characteristics of PFDP **1**, a mixture of di- (**4**) and monobromomethylated (**5**) intermediates was also prepared by varying the ratio of reagents in the preparation step.[21] When reacted with C_{60}, this mixture resulted in macromolecules without $-CH_2Br$ chain ends (denoted PFDP **2**).

MALDI-TOF characterizations (see Figure S4, Supporting Information) confirmed the modification of the C_{60} unit. However, only one unit could be characterized, and this is due to the acknowledged facile rupture of fullerene−methylene bonds.[19b] Gel permeation chromatography (GPC) was used to estimate the distribution of molar masses of the PFDPs. The GPC indicated masses in Figure 1 are considerably less than the actual values because the exclusion volume of C_{60} is much greater than an equivalent molar mass polystyrene standard.[18,19] A very approximate resolution was therefore performed by assuming that each successive peak in the curve of a brut material (obtained directly from the reaction mixture without the precipitation steps that remove lower oligomers) was due to an incremental increase in the number of C_{60}s in the oligomer chain. This is not untoward given the known mechanism of the reaction. The GPC thus indicated that the main components of PFDP **1** and PFDP **2** contained maybe around 10 and 7 C_{60}s, respectively, although this value should be treated with caution. PFDP **2** has a lower average molar mass due to the presence of **5** in its parent mixture. However, both PFDP samples contain large proportions of polymer chains consisting of several tens of repeat units. Aggregates at around 750 s, which disappear on diluting the samples, indicate that the C_{60}s in the PFDPs do not completely lose their THF-phobicity.

An estimation of the content of C_{60} in the PFDPs can be obtained from TGA (Figure S5, Supporting Information).[22] A slight plateau is discerned for both PFDP **1** and PFDP **2** at ca. 450 °C in the degradation curve corresponding to a loss of around 20% weight due to the removal of cyclohexyl ether groups.[23] Degradation at higher temperatures (ca. 600 °C) is due to dexylylation, a dominant process for the shorter PFDP **2**. A plateau observed for PFDP **1** at around 900 °C for ca. 62% remaining weight concords well, within the order of experimental error, with the expected weight ratio of C_{60} in a repeat unit (69%).

The disperse nature of the PFDPs, in that they contained both oligomers and polymers, was supported by differential scanning calorimetry, which showed a broad endothermic melting peak centered around 297 °C (Figure S6, Supporting Information).

^{1}H NMR was used to further elucidate the structure of PFDP **1** and PFDP **2**(see Figure 2). The polymeric nature of the PFDPs and the relatively short chain lengths means that each repeat unit experiences a varied electromagnetic environment. Nevertheless, extremely long experiment time (>48 h) permitted the resolution of major peaks, among the expected spread of minor peaks, rather than the broad curves normally associated with polymers. PFDP **1** exhibits double doublets centered around 4.17 ppm (J = 125.6 Hz, 12.8 Hz) due to diastereotopic C_{60}-methylene protons.[24−26] These are attributed to the asymmetrical 1,4-addition product as this environment provokes a strong inequality in the magnetic environments of the methylene protons. The radical nature of the attacking group makes possible the formation of a 1,2-addition product.[19] However, the steric bulk of the adjacent biscyclohexylether phenylene methylene groups would tend to suggest that such a product would be disfavored. Only PFDP **1** exhibited a quadruplet centered around 4.43 ppm (J = 9.6 Hz) due to $-CH_2Br$ groups. The diastereotopic bromomethylene protons show conformationally restricted interactions with neighboring $-CH_2-O-$ protons. Accordingly, the latter group also gave rise to a finely split double doublet at 3.94 ppm. This effect was not observed for PFDP **2**, confirming the prior attributions of peaks for $-CH_2Br$ and $-CH_2O-$ groups and hence their position in the PFDP **1** structure. The most comparable and discrete peaks were used to derive a ratio of in-chain and chain-end $-CH_2O-$ protons, respectively, at 3.94 and ca. 3.9 ppm indicated that for PFDP **1** there were on average 10.6 in-chain

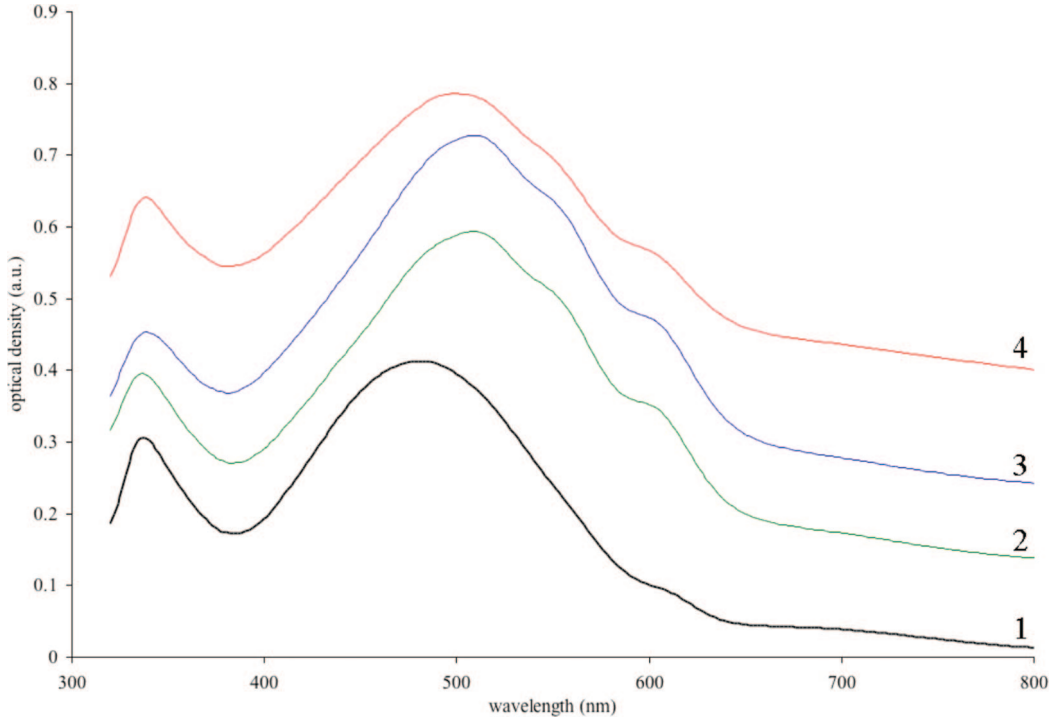

Figure 5. Vertically shifted UV−visible characterizations of thin solid films of active layers made from: (1) P3HT-*blend*-PFDP **1** (1:0.5 respective wt ratio) unannealed; (2) P3HT-*blend*-PCBM (1:0.5 respective wt ratio) annealed at 110 °C; (3) P3HT-*blend*-PFDP **1** (1:0.25 respective wt ratio) annealed at 120 °C; and (4) P3HT-*blend*-PFDP **1** (1:0.5 respective wt ratio) annealed at 120 °C.

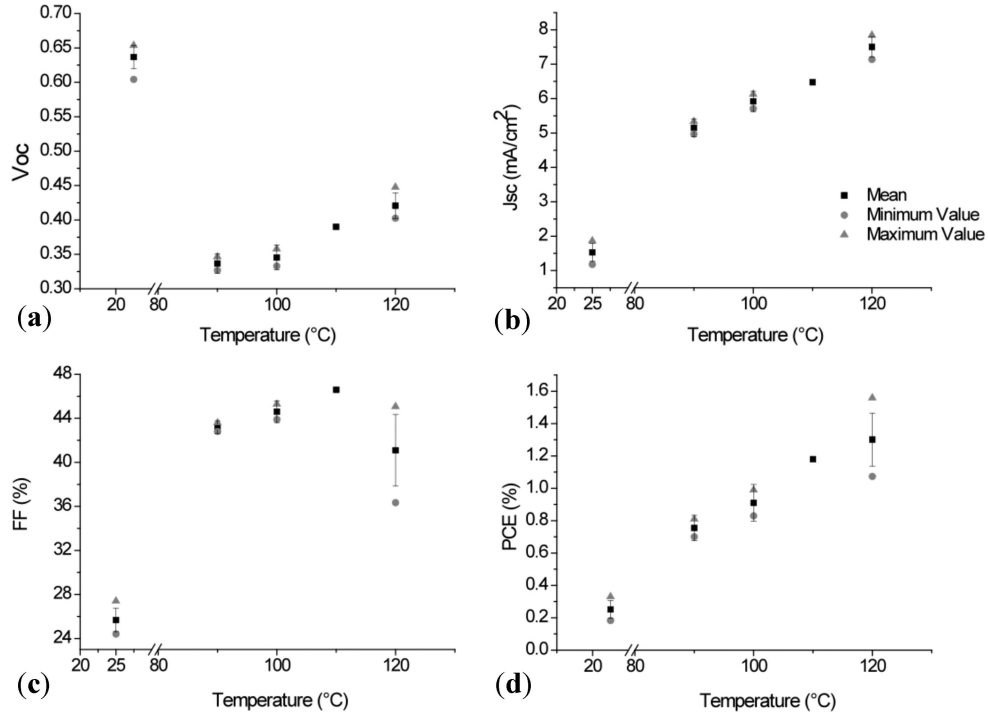

Figure 6. Changes in photovoltaic activity of P3HT-*blend*-PFDP **1** (1:0.5 wt/wt ratio) with annealing temperature in terms of (a) V_{oc}; (b) FF; (c) J_{sc}; and (d) η.

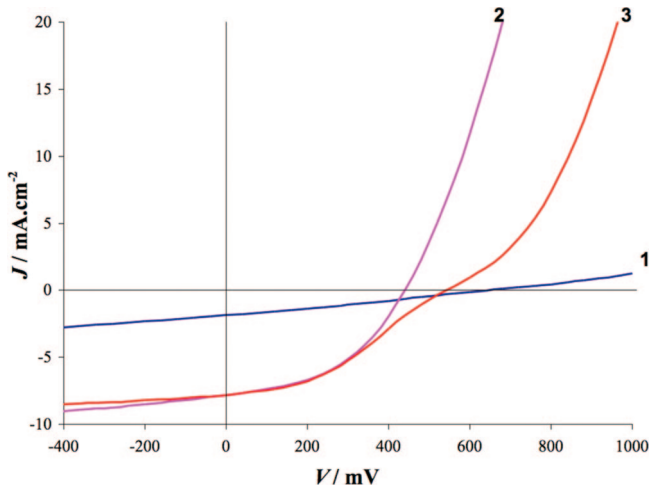

Figure 7. Current density versus voltage for layers of P3HT-*blend*-PFDP **1**: (1) unannealed device; (2) 120 °C after cathode deposition; and (3) 120 °C before and after cathode deposition.

groups for 4 chain-end $-CH_2O-$, equivalent to around 6 C_{60}s per chain. Within the error of the experiment, this value is in agreement with those obtained from the GPC characterizations; however, the result should be treated with caution given the variations in relaxations that occur with steric restrictions. While the presence of tetra-additions to the C_{60} could not be completely excluded, the above results, in accordance with the known mechanism for this reaction,[18,19] indicate a linear-chain structure.

The UV−visible characterization shown in Figure 3 indicated a broad peak around 450 nm that may be considered diagnostic of an 1,4-addition product,[25] corroborating the results from the ^{1}H NMR. Interestingly, the curve closely follows that of what can be considered a model compound (1,4-bis benzyl fullerene) for the PFDPs, which itself also follows quite closely that of C_{60}.[26b] The UV curve results further corroborate the structural identification through the appearance of minor, broad peaks at ca. 600 and 690 nm associated with both 1,4- and 1,2-bis adducts.[24]

PFDP **2** was found, as shown in Figure 4, to undergo fully reversible cyclic voltammetry. The pulse voltammogram indicated two in-chain isomers (Table 1). The major component showed throughout an anodic shift with respect to C_{60} of 150 mV, whereas the minor fraction closely followed C_{60} until the fifth reduction where a discrete peak displays an anodic shift of the order of 306 mV. In general, 1,4-addition products are more facilely reduced than their 1,2-equivalents.[27] The integration over the 5 pairs of reductions would tend to indicate that PFDP **2** consists of ca. 80% of 1,4- and ca. 20% 1,2-addition products, making it a regio-irregular polymer. This result tends to corroborate the aforementioned UV−visible characterisations. Given the small amount of 1,2-addition product present, an indication of its presence in the UV−visible spectra at ca. 430 nm[24] would not be expected to be visible. The estimated electron affinity (LUMO energy level) of PFDP **2** is -4.05 ± 0.05 eV from the onset potential of the first reduction peak at -0.35 V versus a saturated calomel electrode (SCE). It is a value just above that of PCBM (-4.3 eV), and therefore reasonably placed for photovoltaic applications.[28]

Both PFDP **1** and PFDP **2** were tested as blends with commercially available P3HT in photovoltaic devices that were annealed after cathode deposition. Over the ranges of concentration and annealing temperatures used, PFDP **1** gave better results than PFDP **2** (which did not reach an efficiency above 0.6%). This is due to the increased chain length and, possibly, solubility provided by $-CH_2Br$ chain ends. When equivalent weights of P3HT and PFDP **1** were used, efficiencies (η) were low (ca. 0.1%). The UV−visible characterization of the solid film indicated by way of the low value of λ_{max} at 460 nm that this was due to disruption of the crystallization of P3HT. Increasing the ratio of P3HT:PFDP **1** to 1:0.5 and then to 1:0.25 permitted an evolution of the λ_{max} to 500 and 506 nm, respectively, and an increment in the interchain absorptions at ca. 550 and 600 nm (Figure 5). The latter indicate the formation of an extended aggregation

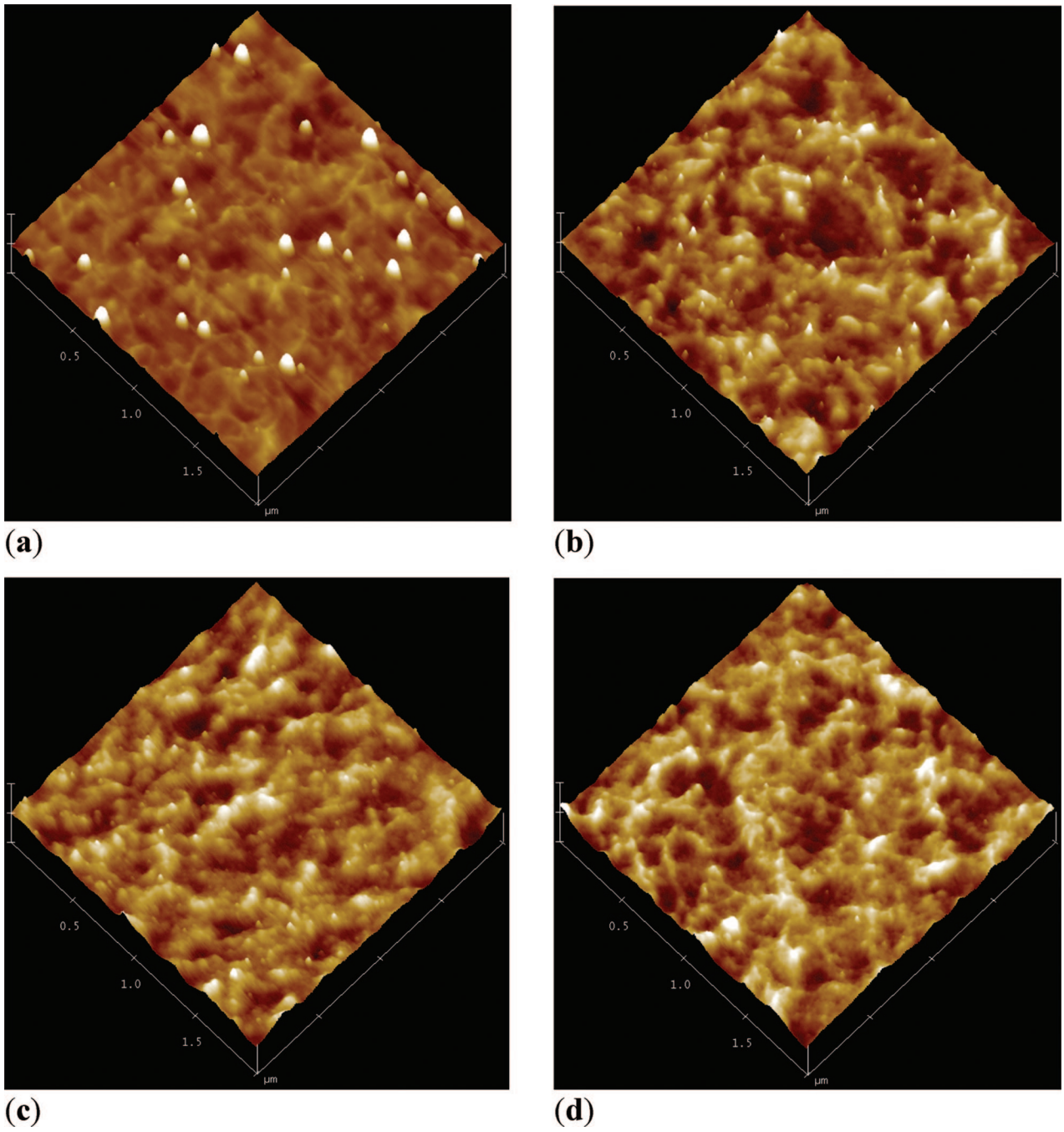

Figure 8. AFM tapping mode height images of a 2.0 × 2.0 μm^2 surface of dried spin-cast films of P3HT-*blend*-PFDP **1** (1:0.5 wt ratio) outside of cathode: (a) prior to annealing (image height = 80 nm); (b) annealed at 90 °C (image height = 40 nm); (c) annealed at 100 °C (image height = 40 nm); and (d) annealed at 110 °C (image height = 40 nm).

of crystalline P3HT.[29−32] Qualitatively speaking, these absorptions are not as important as those obtained for P3HT mixed with PCBM;[29] it is apparent that any future modifications of this prototype PFDP will have to ensure that structuration of the partner polymer is not restricted. Although the respective ratio of 1:0.25 was thus indicated to have the highest degree of P3HT organization, η was limited to 0.4% by a low short circuit current (J_{sc}) at 2.6 mA cm^{-2}, most probably because there was not enough PFDP to ensure exciton capture and charge transfer. Figure 6 shows the characterization of the best ratio of P3HT-*blend*-PFDP **1** (1:0.5) against annealing temperature. The open circuit voltage (V_{oc}) initially decreases with annealing due to a reduction in the P3HT band gap caused by increased self-organization.[29] The V_{oc} then increases as per J_{sc}, the fill factor (FF), and η, indicative of the concomitant and constructive organization of both P3HT and PFDP **1** throughout the device. In all curves, the optimal annealing temperature is around 110 °C where consistent values of η were obtained at around 1.2%. At 120 °C, the devices showed greater deviations with η varying from ca. 1.0% to 1.6%. The FF decreased at 120 °C due to a slight "counter diode" (the bump in the underlying curve 3 shown in Figure 7) that is explained by morphological changes at the electrode interface decreasing carrier selectivity.[33] Similar morphological effects at the cathode may explain why, in general, the V_{oc} is slightly lower than what would be expected from looking at the cyclic voltammetry results alone.

The surface of P3HT-*blend*-PFDP **1** presents an extraordinary behavior on annealing. AFM images (Figure 8 and Figure S7, Supporting Information) show striking, hard nodules about 100 nm tall by 30 nm wide of PFDP **1** in a softer matrix

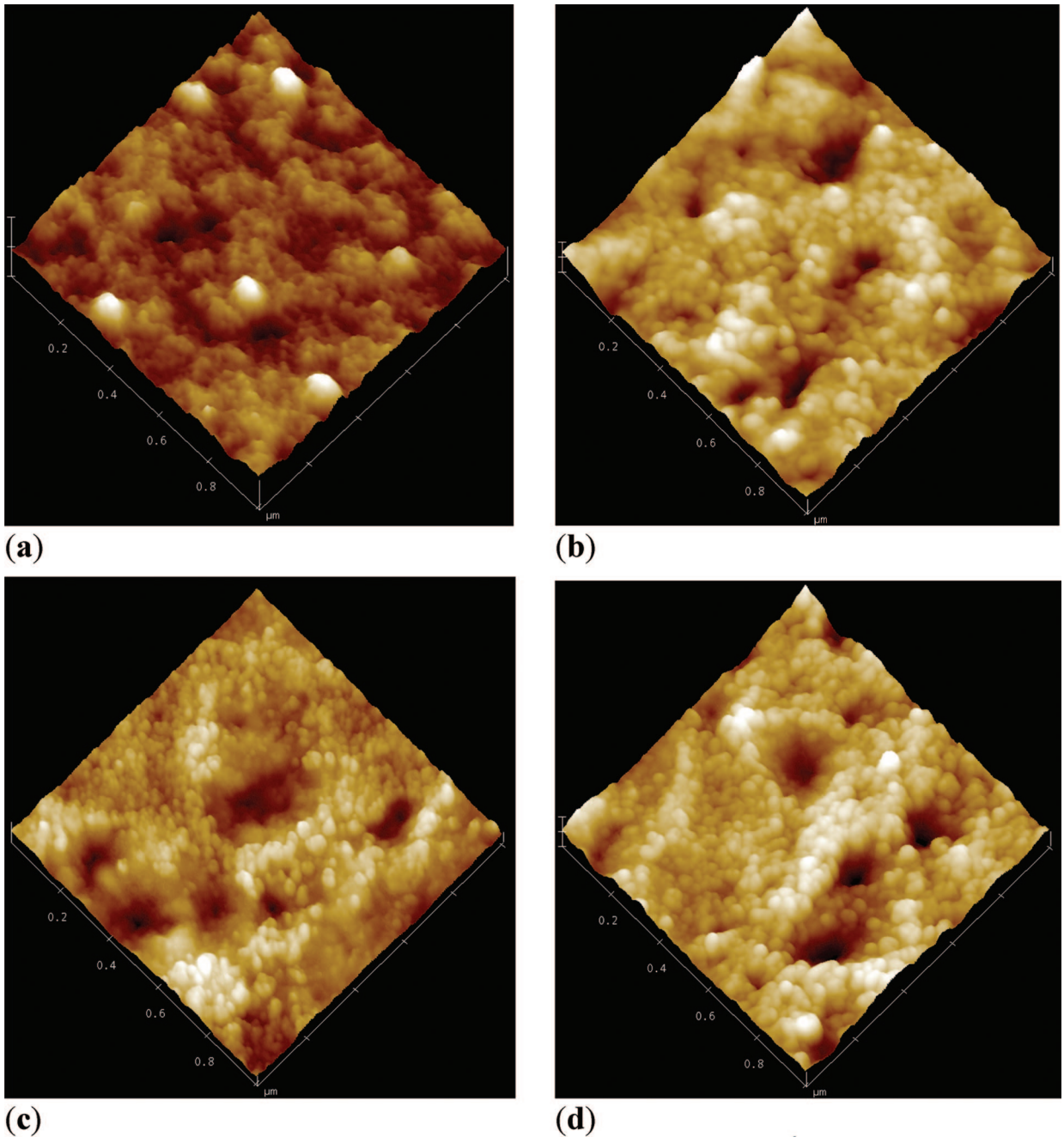

Figure 9. AFM tapping mode height images of a 1.0 × 1.0 μm^2 surface of aluminum-stripped dried spin-cast films of P3HT-*blend*-PFDP **1** (1.0:0.5 weight ratio, all images at 30 nm overall height): (a) prior to annealing; (b) annealed at 90 °C; (c) annealed at 100 °C; and (d) annealed at 110 °C.

of amorphous and fibrillar (ca. 10−20 nm wide) P3HT, as confirmed by phase images. Annealing disperses these primary nodules as the PFDP **1** reptates to reduce the mean surface roughness (R_a) from 2.7 at 25 °C to 2.0 nm at 110 °C. Otherwise, the general features of the P3HT matrix are retained. A more dramatic process was observed below the electrode; Figure 9 shows images taken following cathode removal with "sticky tape", a now well-established technique.[2] With annealing there is the same dispersion of the primary nodules, but now newly formed secondary nodules (ca. 2 nm high by 20−30 nm wide) are distinctly visible at the surface. This difference between surfaces outside and below the cathode indicates that the cathode exerts some capillary, thermal, or chemical effect on the movement of PFDP **1**. It should be stated that in our work there is no depth profiling of the devices. However, the presence of a vertical distribution of PCBM in P3HT-*blend*-PCBM, concentrated toward the cathode, has been demonstrated,[4] and although surprising it should not be untoward that a similar preference occurs for PFDP **1**.

The formation of secondary PFDP **1** nodules explains the increase in the photovoltaic activity as their domain size is closer to that required for exciton capture. More importantly, it is observed that the PFDP does not undergo the crystallization process that can be detrimental to the operation of P3HT-*blend*-PCBM devices.[34]

The detrimental morphological effects that occur on annealing at 120 °C were studied more closely by annealing both prior to and again following deposition of the electrode so as to exacerbate this effect. The tapping mode height AFM in Figure 10a shows the surface outside of the electrode, whereas Figure 10b shows the surface under the electrode. Comparable tapping mode phase images are shown in Figure

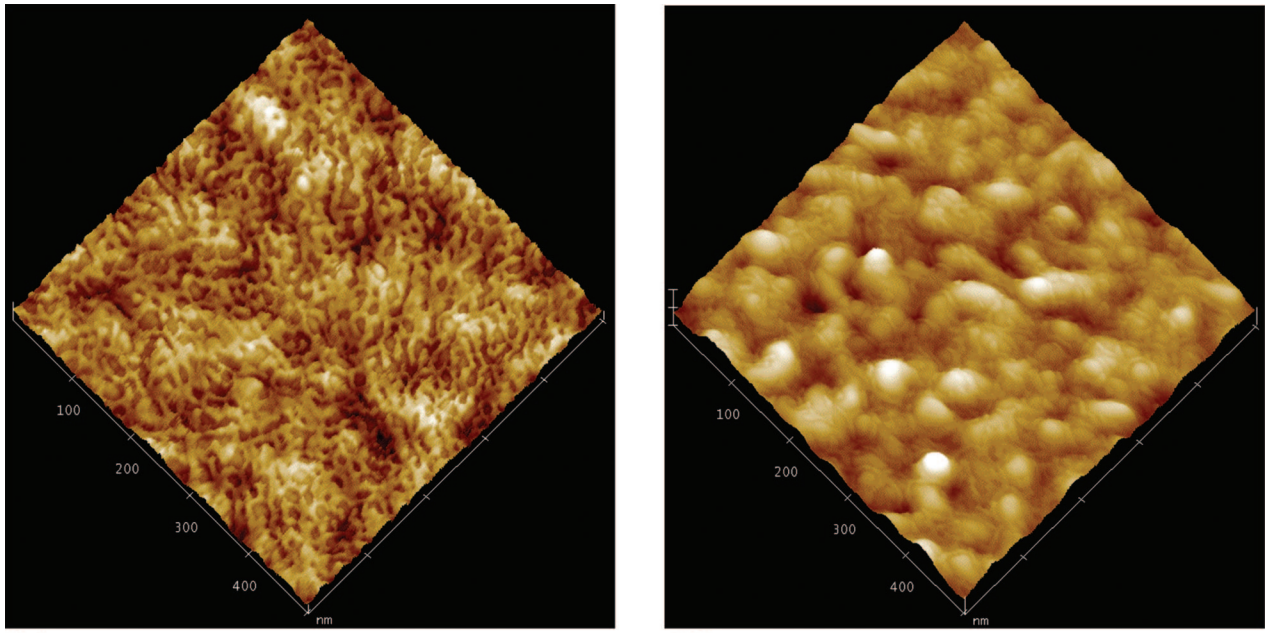

Figure 10. AFM tapping mode height images of a 0.5 × 0.5 μm^2 surface of dried spin-cast films of P3HT-*blend*-PFDP **1** (1.0:0.5 weight ratio): (a) annealed twice at 120 °C under N_2 (height = 4 nm); and (b) annealed at 120 °C under N_2 and then under cathode and then stripped (height = 15 nm).

Table 1. Summary of the Attributed Reduction Peaks of PFDP 2 and of C_{60} versus SCE

PFDP **2**	peak 1 (V)	peak 2 (V)	peak 3 (V)	peak 4 (V)	peak 5 (V)
1,4-addition product	−0.51	−0.92	−1.42	−1.91	−2.41
1,2-addition product	−0.66	−1.10	−1.63	−2.10	−2.25
C_{60}	−0.65	−1.08	−1.57	−2.06	−2.57

S8 of the Supporting Information. It is apparent in the former that there is now a well-defined phase separation of P3HT and PFDP **1** driven by the increase in annealing time and temperature. In the latter image, there is a wall with ripped edges of P3HT, around 2 nm thick, at the base of each nodule. This indicates that there was a layer of P3HT next to the electrode and between the PFDP **1** nodules. The result is confirmed by the appearance of a counter-diode effect when the diode is annealed heated to 120 °C both before and after cathode deposition (Figure 7, curve 3). It is therefore probable that at high temperatures, coinciding with the second glass transition temperature of P3HT at 120 °C, through entropic effects, amorphous low molar mass P3HT inserts itself between the cathode and the PFDP **1** to decrease the FF.

Conclusion

This work has demonstrated that an original class of high C_{60} content polymers is extremely accessible. Importantly, the facile nature of the synthesis means that the reaction may be easily scalable. It is expected that variations in the inter-C_{60} moiety will permit great variations in solubilities, mixing characteristics with the electron donor polymer partner, and opto-electronic properties. However, the corresponding reagents will require steric bulk to ensure that multiple additions to the C_{60}, and hence cross-linking reactions, do not occur. It is probable that higher chain lengths may be obtained through further optimization of the reaction conditions and times. It is interesting to note that the chain ends of PFDP **1** may lend themselves to further chemistry, albeit that which is determined to an extent by the presence of the reactive C_{60}. The very promising initial and unoptimized characterizations of P3HT-*blend*-PFDP have demonstrated, even with a prototype PFDP chemical structure, that these materials are of further interest for photovoltaic activities, especially given their extremely novel behavior that is quite unlike PCBM. Future work may now look to increasing the molecular weights and varying the inter-C_{60} moiety.

Experimental Section

Instrumentation. ^1H (400 MHz) and ^{13}C (100 MHz) NMR spectra were recorded on a Bruker Avance 400 spectrometer at ambient temperature. Gel permeation chromatography (GPC) was performed using THF as eluant at 35 °C and a flow rate of 1 mL min^{-1} through four columns (TSK G5000HXL (9 μm), G4000HXL (6 μm), G3000HXL (6 μm), and G2000HXL (5 μm)) and connected to a Varian refractometer and UV−visible spectrophotometer. TGA was performed with a Perkin-Elmer TGA 7 Thermogravimetric Analyzer from 30 to 600 °C at a heating rate of 10 °C min^{-1} and under nitrogen. DSC was performed on a TA DSC Q100 series calorimeter from TA Instruments under nitrogen at scan rates of 10 °C min^{-1}, and data were collected on a second heating scan. UV−visible absorption spectra were obtained at ambient temperature from solutions of PFDP in toluene (at a concentration of 0.106 g L^{-1}, equivalent to ca. 1.5 × 10^{-5} M) using a Varian Cary 100 Scan UV−visible spectrophotometer.

Atomic force microscopy (AFM) was performed under air at 25 °C using a Nanoscope IIIa microscope in tapping mode. Commercially available silicon tip probes had a spring constant of 42 N m^{-1}, a resonance frequency of 285 kHz, and a typical radius of curvature in the 8−10 nm range. Both topography and phase signal images were recorded with 512 × 512 data points.

Electrochemical experiments were performed under nitrogen at ambient temperature using a platinum disk working electrode (diameter = 1.6 mm), a platinum wire as the counter electrode, and a silver wire as a pseudo-reference electrode. The three-electrode cell was connected to an Autolab PGSTAT100 potentiostat. C_{60} and PFDP **2** were both characterized as 1 mg mL^{-1} solutions in toluene/acetonitrile (4:1) with tetrabutylammonium hexafluorophosphate (0.1 M) as a supporting electrolyte. Ferrocene was added to the electrolyte solution at the end of a

series of experiments so that the ferrocene/ferrocenium (Fc/Fc^+) couple served as an internal standard. The Fc/Fc^+ couple standard potential was measured at 0.49 V versus the saturated calomel electrode (SCE) under the same experimental conditions. All potentials in the tables and figures are referred to the SCE. Cyclic voltammetry measurements were carried out at 0.1 V s^{-1}, and pulse voltammetry was performed using 0.05 s as modulation time and 25 mV as the pulse amplitude. The electron affinity (EA) or lowest unoccupied molecular orbital (LUMO) was estimated from the redox data. The LUMO level was calculated using E_{LUMO} (eV) = $-[E_{onset\ red}$ (versus SCE) + 4.4] based on an SCE energy level of 4.4 eV relative to vacuum.

All bulk heterojunction photovoltaic cells were prepared using solutions of P3HT:PFDP in respective wt/wt ratios varying from 1:1 to 1:0.25, and based on concentrations of P3HT in anhydrous chlorobenzene at 15 mg mL^{-1}. "Standard" grade regioregular P3HT was obtained from Rieke Metals Inc. The glass−ITO substrates (obtained from PGO, Germany) were sequentially cleaned in an ultrasonic bath with acetone and isopropanol, rinsed with deionized water, dried in an oven at 100 °C for 60 min, and treated with UV-ozone. The substrate was spin-coated with poly(3,4-ethylenedioxythiophene)-*blend*-poly(styrene sulfonate) (PEDOT-*blend*-PSS) (Baytron P) at 1500 rpm, and oven-dried at 140 °C for 60 min to give a ca. 40 nm film. The active layer was deposited by spin-casting from an anhydrous chlorobenzene solution under dry nitrogen to obtain films 80−90 nm thick. Following drying under reduced pressure at 2×10^{-7} mbar for 1 h, the devices were completed by deposition of the Ca/Al (20 and 80 nm, respectively) cathode in that order through a shadow mask with 6 mm diameter openings at ca. 2×10^{-7} mbar. All cells had a 28 mm^2 active surface. The annealing process was carried out under an inert atmosphere by placing the cells or films deposited on glass directly onto a controlled hot plate. A minimum of six devices were prepared for each annealing temperature for all blends considered. Cell performances were evaluated following free cooling to ambient temperature. Current−voltage characteristics and power conversion efficiencies of the solar cells were measured in inert atmosphere via a computer-controlled Keithley SMU 2400 unit using 100 mW cm^{-2} air-mass (1.5) simulated white light developed by a Steuernagel Solar Constant 575 simulator. The mismatch factor was not taken into account; however, this standard setup gave a Class AAA spectral mismatch (to a factor of $<\pm 25\%$) up to 700 nm, which covered the spectral absorption range of PFDP and P3HT. The calculation of the power conversion efficiency (η) of the photovoltaic cells was as detailed elsewhere.[29]

Materials. All materials were used as obtained from commercial sources. Solvents were distilled from over their respective drying agents under dried nitrogen. All reactions were performed in flame-dried and dry nitrogen flushed glassware. 1,4-Bis(methylcyclohexyl ether) benzene (**3**), 1,4-bis(methylcyclohexyl ether)-2,5-dibromomethyl benzene (**4**), and 1,4-bis-(methylcyclohexyl ether)-2-bromomethyl benzene (**5**) were prepared following protocols in ref 21 and detailed in the Supporting Information.

Synthesis of α,ω-Bromomethyl-poly{(1,4-fullerene)-*alt*-[1,4-dimethylene-2,5-bis(cyclohexylmethyl ether)phenylene]} (PFDP 1). This is a representative method for PFDP samples. In a 1000 mL vessel, C_{60} (500 mg, 6.94×10^{-4} mol) and **4** (0.2699 g, 5.552×10^{-4} mol) in a respective ratio of 1:0.8 were dissolved in toluene (250 mL) at room temperature. CuBr (0.876 g, 6.11×10^{-3} mol, 5.5 equiv with respect to $-CH_2Br$ groups on **4**) and bipyridine (2.098 g, 1.343×10^{-2} mol, 2.2 equiv to CuBr) were added, and the temperature of the vigorously stirred mixture was slowly raised to 115 °C. After 22 h under cover from light, the mixture was reduced to ca. 100 mL by evaporation and dropped into THF (700 mL) to precipitate unreacted fullerene. Precipitates and CuBr were then removed by passing the solution through a ca. 20 cm column of silica gel (MN Kieselgel 60M, 230−400 mesh), and the red solution again reduced to around 200 mL by evaporation. The product was then recovered following three precipitations in methanol (700 mL), first from the THF solution, then from a solution in toluene (ca. 100 mL). This process removed unreacted **4** and the shortest PFDPs, as indicated by the difference in GPCs of the brut and purified samples. The light brown product was dried under reduced pressure for 3 d at 40 °C (yield 31% with respect to C_{60}). ^1H NMR (400 MHz, C_6D_6, ambient temperature): 6.87 (phenyl−H), 4.43 (AB quartet, $J = 9.6$ Hz, $-CH_2-Br$), 4.17 ($J = 125.6$ Hz, 12.8 Hz, 1,4-$C_{60}-CH_2-$), 3.94 (dd, $J = 6$ Hz, 1.3 Hz, in-chain $-O-CH_2-$), 3.91, 3.89, 3.88, 3.87 (four last peaks due to chain end $-O-CH_2-$), and broad peaks from 2.1 to 1.5 and 1.45 to 0.8 ppm (cyclohexyl−H). ^{13}C NMR was attempted, but peaks due to C_{60} were poorly defined, even after using long interpulse times and numerous scans, due to conformational restrictions and relatively low concentrations.

Acknowledgment. Séverine Bailly, Pascal Maisse, Christiane Vitry, and Nicolas Guidolin are gratefully thanked for technical assistance. Thanks are extended to the CNRS and the ANR through the "SOLCOP" research program, for funding R.C.H.

Supporting Information Available: Complete syntheses of **3**−**5** and PFDP **2**, ^1H and ^{13}C NMR spectra of **3**, **4**, and **4** mixed with **5**, MALDI-TOF of PFDP **2**, TGA of PFDP **1** and PFDP **2**, DSC curves of PFDP **1**, and complementary AFM tapping mode phase images of P3HT-*blend*-PFDP **1** (1:0.5 wt ratio). This material is available free of charge via the Internet at http://pubs.acs.org.

References and Notes

(1) (a) Günes, S.; Neugebauer, H.; Sariciftci, N. S. *Chem. Rev.* **2007**, *107*, 1324. (b) Thompson, B. C.; Fréchet, J. M. J. *Angew. Chem., Int. Ed.* **2008**, *47*, 58.
(2) Ma, M.; Yang, C.; Gong, X.; Lee, K.; Heeger, A. J. *Adv. Funct. Mater.* **2005**, *15*, 1617.
(3) Nunzi, J.-M. *C. R. Physique* **2002**, *3*, 523.
(4) Campoy-Quiles, M.; Ferenczi, T.; Agostinelli, T.; Etchegoin, P. G.; Kim, Y.; Anthopoulos, T. D.; Stavrinou, P. N.; Bradley, D. D. C.; Nelson, J. *Nat. Mater.* **2008**, *7*, 158.
(5) Yang, X.; Loos, J.; Veenstra, S. C.; Verhees, W. J. H.; Wienk, M. M.; Kroon, J. M.; Michels, M. A. J.; Janssen, R. A. J. *Nano Lett.* **2005**, *5*, 579.
(6) Yu, G.; Heeger, A. J. *J. Appl. Phys.* **1995**, *78*, 4510.
(7) Halls, J. J. M.; Walsh, C. A.; Greenham, N. C.; Marseglia, E. A.; Friend, R. H.; Moratti, S. C.; Holmes, A. B. *Nature (London)* **1995**, *376*, 498.
(8) Sun, S.-S.; Zhang, C.; Ledbetter, A.; Choi, S.; Seo, K.; Bonner, C. E., Jr.; Drees, M.; Sariciftci, N. S. *Appl. Phys. Lett.* **2007**, *90*, 043117.
(9) (a) Jaiswal, M.; Menon, R. *Polym. Int.* **2006**, *55*, 1371. (b) Moliton, A.; Hiorns, R. C. *Polym. Int.* **2004**, *53*, 1397.
(10) (a) Barrau, S.; Heiser, T.; Richard, F.; Brochon, C.; Ngov, C.; van de Wetering, K.; Hadziioannou, G.; Anokhin, D. V.; Ivanov, D. A. *Macromolecules* **2008**, *41*, 2701. (b) Adamopoulos, G.; Heiser, T.; Giovanella, U.; Ould-Saad, S.; van de Wetering, K.; Brochon, C.; Zorba, T.; Paraskevopoulos, K. M.; Hadziioannou, G. *Thin Solid Films* **2006**, *511*−*512*, 371. (c) Heiser, T.; Adamopoulos, G.; Brinkmann, M.; Giovanella, U.; Ould-Saad, S.; Brochon, C.; van de Wetering, K.; Hadziioannou, G. *Thin Solid Films* **2006**, *511*−*512*, 219.
(11) (a) Sivula, K.; Ball, Z. T.; Watanabe, N.; Fréchet, J. M. J. *Adv. Mater.* **2006**, *18*, 206. (b) Ball, Z. T.; Sivula, K.; Fréchet, J. M. J. *Macromolecules* **2006**, *39*, 70.
(12) Drees, M.; Hoppe, H.; Winder, C.; Neugebauer, H.; Sariciftci, N. S.; Schwinger, W.; Schäffler, F.; Topf, C.; Scharber, M. C.; Zhu, Z.; Gaudiana, R. *J. Mater. Chem.* **2005**, *15*, 5158.
(13) (a) Lindner, S. M.; Hüttner, S.; Chiche, A.; Thelakkat, M.; Krausch, G. *Angew. Chem., Int. Ed.* **2006**, *45*, 3364. (b) Sommer, M.; Lang, A. S.; Thelakkat, M. *Angew. Chem., Int. Ed.* **2008**, *47*, 7901. (c) Sommer, M.; Hüttner, S.; Wunder, S.; Thelakkat, M. *Adv. Mater.* **2008**, *20*, 2523. (d) Zhang, Q.; Cirpan, A.; Russell, T. P.; Emrick, T. *Macromolecules* **2009**, *42*, 1079.
(14) Giacalone, F.; Martín, N. *Chem. Rev.* **2006**, *106*, 5136.
(15) Gogel, A.; Belik, P.; Walter, M.; Kraus, A.; Harth, E.; Wagner, M.; Spickermann, J.; Müllen, K. *Tetrahedron* **1996**, *52*, 5007.
(16) Shi, S.; Khemani, K. C.; Li, Q. "C"; Wudl, F. *J. Am. Chem. Soc.* **1992**, *114*, 10656.
(17) Ito, H.; Ishida, Y.; Saigo, K. *Tetrahedron Lett.* **2006**, *47*, 3095.

(18) Mathis, C.; Schmaltz, B.; Brinkmann, M. *C. R. Chimie* **2006**, *9*, 1075.
(19) (a) Audouin, F.; Nuffer, R.; Mathis, C. *J. Polym. Sci., Part A: Polym. Chem.* **2004**, *42*, 3456. (b) Pozdnyakov, O. F.; Pozdnyakov, A. O.; Schmaltz, B.; Mathis, C. *Polymer* **2006**, *47*, 1028. (c) Hiorns, R. C.; Iratçabal, P.; Bégué, D.; Khoukh, A.; Bettignies, R.; Leroy, J.; Firon, M.; Sentein, C.; Martinez, H.; Preud'homme, H.; Dagron-Lartigau, C. *J. Polym. Sci., Part A: Polym. Chem.* **2009**, *47*, 2304.
(20) Skiebe, A.; Hirsch, A. *J. Chem. Soc., Chem. Commun.* **1994**, 335.
(21) van der Made, A. W.; van der Made, R. H. *J. Org. Chem.* **1993**, *58*, 1262.
(22) (a) Cloutet, E.; Gnanou, Y.; Fillaut, J.-L.; Astruc, D. *Chem. Commun.* **1996**, 1565. (b) Cloutet, E.; Fillaut, J.-L.; Astruc, D.; Gnanou, Y. *Macromolecules* **1999**, *32*, 1043.
(23) Chambon, S.; Rivaton, A.; Gardette, J.-L.; Firon, M. *Sol. Energy Mater. Sol. Cells* **2007**, *91*, 394.
(24) Kadish, K. M.; Gao, X.; Van Caemelbecke, E.; Suenobu, T.; Fukuzumi, S. *J. Phys. Chem. A* **2000**, *104*, 3878.
(25) Kadish, K. M.; Gao, X.; Van Caemelbecke, E.; Hirasaka, T.; Suenobu, T.; Fukuzumi, S. *J. Phys. Chem. A* **1998**, *102*, 3898.
(26) (a) Subramanian, R.; Kadish, K. M.; Vijayashree, M. N.; Gao, X.; Jones, M. T.; Miller, M. D.; Krause, K. L.; Suenobu, T.; Fukuzumi, S. *J. Phys. Chem.* **1996**, *100*, 16327. (b) Miki, S.; Kitao, M.; Fukunishi, K. *Tetrahedron Lett.* **1996**, *37*, 2049.
(27) Kadish, K. M.; Gao, X.; Van Caemelbecke, E.; Suenobu, T.; Fukuzumi, S. *J. Am. Chem. Soc.* **2000**, *122*, 563.
(28) (a) Scharber, M. C.; Mühlbacher, D.; Koppe, M.; Denk, P.; Waldauf, C.; Heeger, A. J.; Brabec, C. J. *Adv. Mater.* **2006**, *18*, 789. (b) D'Andrade, B. W.; Datta, S.; Forrest, S. R.; Djurovich, P.; Polikarpov, E.; Thompson, M. E. *Org. Electron.* **2005**, *6*, 11. (c) Leeuw, D. M.; Simeon, M. M. J.; Brown, A. R.; Einerhand, R. E. F. *Synth. Met.* **1997**, *87*, 53.
(29) Hiorns, R. C.; de Bettignies, R.; Leroy, J.; Bailly, S.; Firon, M.; Sentein, C.; Khoukh, A.; Preud'homme, H.; Dagron-Lartigau, C. *Adv. Funct. Mater.* **2006**, *16*, 2263.
(30) Saunders, B. R.; Turner, M. L. *Adv. Colloid Interface Sci.* **2008**, *138*, 1.
(31) Liu, J.; Loewe, R. S.; McCullough, R. D. *Macromolecules* **1999**, *32*, 5777.
(32) (a) Kline, R. J.; McGehee, M. D.; Kadnikova, E. N.; Liu, J.; Fréchet, J. M. J.; Toney, M. F. *Macromolecules* **2005**, *38*, 3312. (b) Brinkmann, M.; Rannou, P. *Macromolecules* **2009**, *42*, 1125.
(33) Brabec, C. J.; Cravino, A.; Meissner, D.; Sariciftci, N. S.; Fromherz, T.; Rispens, M. T.; Sanchez, L.; Hummelen, J. C. *Adv. Funct. Mater.* **2001**, *11*, 374.
(34) Swinnen, A.; Harldermans, I.; vande Ven, M.; D'Haen, J.; Vanhoyland, G.; Aresu, S.; D'Olieslaeger, M.; Manca, J. *Adv. Funct. Mater.* **2006**, *16*, 760.

MA900279A